



Optical Linear Polarization toward the Open Star Cluster Casado Alessi 1

Sadhana Singh¹, Jeewan C. Pandey¹ , R. K. S. Yadav¹, and Biman J. Medhi^{1,2}

¹ Aryabhata Research Institute of Observational Sciences (ARIES), Manora Peak, Nainital 263001, India; ssingh@aries.res.in, jeewan@aries.res.in

² Gauhati University, Guwahati 781014, India

Received 2019 October 30; revised 2019 December 4; accepted 2019 December 24; published 2020 February 11

Abstract

We present B -, V -, R -, and I -band linear polarimetric observations of 73 stars in the direction of open star cluster Casado Alessi 1 (hereafter Alessi 1). We aim to use polarimetry as a tool to investigate the properties and distribution of dust grains toward the direction of the cluster. The polarimetric observations were carried out using the ARIES IMaging POLarimeter mounted at the 104 cm telescope of ARIES, Nainital (India). Using the *Gaia* photometric data the age and distance of the cluster are estimated to be 0.8 ± 0.1 Gyr and 673 ± 98 pc, respectively. A total of 66 stars with a $26'$ radius from the cluster are identified as members of the cluster using the astrometric approach. Out of these 66 members, 15 stars were observed polarimetrically and found to have the same value of polarization. The majority of the stars in the region follow the general law of polarization for the interstellar medium, indicating that polarization toward the cluster Alessi 1 is dominated by foreground dust grains. The average values of the maximum polarization (P_{\max}) and the wavelength corresponding to the maximum polarization (λ_{\max}) toward the cluster are found to be $0.83 \pm 0.03\%$ and $0.59 \pm 0.04 \mu\text{m}$, respectively. Also, dust grains toward the cluster appear to be aligned, possibly due to the galactic magnetic field.

Unified Astronomy Thesaurus concepts: [Interstellar medium \(847\)](#); [Interstellar dust \(836\)](#); [Open star clusters \(1160\)](#); [Polarimetry \(1278\)](#); [Starlight polarization \(1571\)](#); [Interstellar dust extinction \(837\)](#)

1. Introduction

The presence of dust grains in the interstellar medium (ISM) can be revealed by interaction with starlight and then further emission/scattering from the dust grains, which in turn produce polarized light. The dichroic extinction of starlight by aligned asymmetric dust grains in the ISM is considered the main source of ISM polarization. Although the identity of the dominant grain alignment mechanism has proved to be an intriguing problem in grain dynamics (Lazarian et al. 1997; Lazarian 2003; Voshchinnikov 2012), it is generally believed that asymmetric grains tend to become aligned to the local magnetic field through the grains shortest axis parallel to the magnetic field (Davis & Greenstein 1951). Thus, linear polarimetric observations may provide information about the geometry of the underlying magnetic field of the region. This will shed light on the observed region's type, e.g., whether it is star-forming, a dense molecular cloud, etc. (see Heiles 1996; Lazarian 2007; Frisch et al. 2018). The wavelength dependence of polarization gives information about the size distribution of dust grains. The total to selective extinction is thought to be related to the wavelength corresponding to maximum polarization (λ_{\max}) (Whittet & van Breda 1978). Thus, the polarimetric technique is considered a useful tool to explore the properties of dust grains (e.g., Kim & Martin 1994; Vaillancourt et al. 2011). Polarimetric study of open star clusters is useful for determining the properties of foreground interstellar dust, as the majority of the clusters have basic information like distance, membership, color, etc. (e.g., see Feinstein et al. 2008; Medhi et al. 2008).

In this paper, we have studied an open star cluster Alessi 1 [R.A.(J2000) = $00^{\text{h}}53^{\text{m}}27^{\text{s}}$, Decl.(J2000) = $+49^{\circ}34'11''$; $l = 123^{\circ}26$, $b = -13^{\circ}30$] (Kharchenko et al. 2005) using the B -, V -, R -, and I -band polarimetric observations and *Gaia* archival data. According to Alessi et al. (2003), Alessi 1 has a large diameter of $54'$ with an isolated group of stars. They found 28

probable members of the cluster from their kinematic analysis. Using photometric data from the Tycho 2 catalog, they did not find any cluster sequence in the color–magnitude diagram (CMD). Kharchenko et al. (2004) estimated the distance to be 800 pc, the angular radius of core and cluster to be $7'8$ and $27'$, the age to be 0.7 Gyr, and 23 probable members of the cluster. However, Kharchenko et al. (2013) estimated the distance to the cluster to be nearly 750 pc, and found the age of the cluster to be similar to that found by Kharchenko et al. (2004). They also estimated the angular radii of the core, central part, and the cluster for Alessi 1 as $3'$, $10'5$, and $25'5$, respectively. Bossini et al. (2019) estimated age, distance modulus, extinction in the V and G bands as 0.86 Gyr, 9.255 mag, 0.322 mag, and 0.314 mag, respectively, for the cluster Alessi 1. Recently, Cantat-Gaudin et al. (2018) derived the membership probability of 63 stars in this cluster using *Gaia* data, and found 56 stars have membership probabilities greater than 50%.

The paper is organized as follows. The observations and data reduction, along with the archival *Gaia* data, are described in Section 2, and in Section 3, we present our results, analysis and discussion. In Section 4 we summarize our results.

2. Observations and Data Reduction

2.1. Polarimetry

The optical polarimetric observations of the cluster Alessi 1 were carried out on 2017 November 22 and 23 in the B , V , R , and I photometric passbands using the ARIES IMaging POLarimeter (AIMPOL; Rautela et al. 2004) mounted at the Cassegrain focus of the 104 cm Sampurnanand telescope of ARIES, Nainital. The telescope is a Ritchey–Chretien reflector with a focal ratio of $f/13$ (Sinvhal et al. 1972). The detector was a Tek 1k \times 1k charge-coupled device (CCD) camera cooled by liquid nitrogen. Each pixel of the CCD corresponds to $1''.73 \times 1''.73$, resulting in an entire field of view (fov) of CCD of $\sim 8'$ in diameter. The gain and read-out-noise of

the CCD are $11.98 e^-$ per ADU and $7.0 e^-$, respectively. Observations were taken in four positions of the half-wave plate (HWP), α , of 0° , 22.5° , 45° , and 67.5° from north–south to get the linear polarization. There was a 27 pixel separation between the ordinary and extraordinary images of each source in the CCD frame. As the fov of the AIMPOL is small, to observe a large fov for the cluster, we have divided the cluster into seven regions. Thus, we observed a total fov of $\sim 12'$ in radius, which is similar to the radius of the central part of the cluster as estimated by Kharchenko et al. (2013). Three continuous observations were taken in each position of HWP for every region. The exposure times were varied from 50 to 180 s depending upon the filter used. In order to improve the signal-to-noise ratio, we have added all three frames in each position of HWP. Stars HD 19820 and HD 21447 were observed as standard polarized and unpolarized stars, respectively, in the *B*, *V*, *R*, and *I* filters for the calibration on each night of observation.

The Image Reduction and Analysis Facility (IRAF³) was used to perform aperture photometry to get the flux of the extraordinary (I_e) and ordinary (I_o) images of each star in the CCD frame. The ratio $R(\alpha)$ at each position of HWP is given by

$$R(\alpha) = \frac{\frac{I_e}{I_o} - 1}{\frac{I_e}{I_o} + 1} = P \cos(2\theta - 4\alpha), \quad (1)$$

where P is the fraction of total linearly polarized light and θ is the polarization position angle. The error associated with $R(\alpha)$ is given by

$$\sigma_{R(\alpha)} = \frac{\sqrt{I_e + I_o + 2I_b}}{I_e + I_o}, \quad (2)$$

where I_b is average background counts around the extraordinary and ordinary images. As the responses of the CCD to the two orthogonal polarization components may not be the same and are a function of position on its surface, the actual measured signal in the two images may differ from by a factor F as given in

$$F = \sqrt[4]{\frac{I_o(0)}{I_e(45)} \times \frac{I_o(45)}{I_e(0)} \times \frac{I_o(22.5)}{I_e(67.5)} \times \frac{I_o(67.5)}{I_e(22.5)}}. \quad (3)$$

Now, the ratio $R(\alpha)$ is given by

$$R(\alpha) = \frac{\frac{I_e}{I_o} \times F - 1}{\frac{I_e}{I_o} \times F + 1}. \quad (4)$$

Correction for instrumental polarization and zero-point calibration of position angle were done using unpolarized and polarized standard stars, respectively. The instrumental polarization was found to be less than 0.3% in all observed passbands (see also Medhi et al. 2007; Pandey et al. 2009; Eswaraiah et al. 2011; Soam et al. 2015; Patel et al. 2016, etc.). The polarization results for polarized standard stars after the correction of instrumental polarization are given in Table 1 along with the values derived by Schmidt et al. (1992). As the overlapping of an ordinary image with the adjacent extraordinary image cannot be avoided due to the absence of a grid

in the AIMPOL, to take care of target sources we have selected only those isolated stars that do not show any overlapping of the ordinary image with an adjacent extraordinary image. Furthermore, we have considered only those stars that have an error of less than 50% in the degree of polarization and/or position angle. This turned out to be only 73 stars in the observed fov of the cluster Alessi 1. We have performed astrometry of observed sources using CCMAP and CCTRAN packages in IRAF. The rms error in the performed astrometry was around $0''.28$.

2.2. Gaia Archive

We have also used *Gaia* DR2 data (Gaia Collaboration et al. 2016, 2018; Lindegren et al. 2018; Luri et al. 2018) to determine the basic parameters and membership of the cluster Alessi 1. We have extracted the data of the stars within a $26'$ radius of the cluster, which was also the center of the polarimetric observations. We have chosen this radius because the angular radius of the cluster was estimated to be $25.5'$ by Kharchenko et al. (2013). We have taken only those sources from *Gaia* DR2 for which the three conditions for a five parameter (positions, parallax, and proper motions) solution are met (see Lindegren et al. 2018). These conditions are as follows: the mean *G*-band magnitude should be brighter than 21.0 mag, the number of distinct observation epochs should be greater than 6, and the parameter *astrometric_sigma5d_max* $\leq (1.2 \text{ mas}) \times \gamma(G)$, where $\gamma(G) = \max[1, 10^{0.2(G-18)}]$. Sources for which proper motion in R.A. (μ_α) and decl. (μ_δ) were outside the range of -30 to $+30 \text{ mas yr}^{-1}$ were also discarded. After applying the above conditions, a total of 11,004 sources were found in the selected region of the cluster Alessi 1. The parameters, μ_α , μ_δ , parallax, the magnitude in the *G* band (*G*), color ($G_{BP} - G_{RP}$), and color excess [$E(G_{BP} - G_{RP})$] of *Gaia* sources were extracted from the *Gaia* archive for our analysis.

We have cross-matched our observed sources with the *Gaia* sources using the CDS X-Match Service.⁴ We have used positional error cross-match criteria with 5σ for the 100% completeness and maximum distance up to $5''$. Thus, out of 73 polarimetrically observed stars, 68 stars were cross-matched with the *Gaia* sources using these criteria. We found that 44 stars were matched within $1''(1.05\sigma)$ and 7 stars were matched within $1''-2''(2.29\sigma)$, whereas in the offset ranges of $2''-3''(3.48\sigma)$ and $3''-4''(4.58\sigma)$, 9 and 8 stars were matched, respectively.

3. Results, Analysis, and Discussion

The degree of polarization and position angle for 73 stars toward the cluster region in *B*, *V*, *R*, and *I* photometric passbands, along with their *Gaia* IDs, are given in Table 2. In the first column, the serial numbers for all stars are given. *Gaia* ID, distances between observed stars and *Gaia* positions, and distances in terms of σ are given in columns 2–4, respectively, for all 68 cross-matched stars. The degree of polarization and corresponding position angle for all stars in four different filters are given in columns 5–12. For the remaining five stars, R.A. and decl. are listed in the table footnote, along with their serial numbers.

³ <http://iraf.net>

⁴ <http://cdsxmatch.u-strasbg.fr/>

Table 1
Polarization and Position Angles of Polarized Standard Star HD 19820 on Two Different Nights

Passband	Present Work				Schmidt et al. (1992)	
	2017 November 22		2017 November 23		P(%)	$\theta(^{\circ})$
	P(%)	$\theta(^{\circ})$	P(%)	$\theta(^{\circ})$		
<i>B</i>	4.71 ± 0.02	115.8 ± 0.1	4.65 ± 0.10	115.6 ± 0.6	4.699 ± 0.036	115.7 ± 0.2
<i>V</i>	4.76 ± 0.11	114.9 ± 0.6	4.43 ± 0.15	114.8 ± 0.9	4.787 ± 0.028	114.93 ± 0.17
<i>R</i>	4.45 ± 0.11	114.6 ± 0.7	4.43 ± 0.13	114.5 ± 0.8	4.526 ± 0.025	114.46 ± 0.16
<i>I</i>	3.94 ± 0.07	114.4 ± 0.5	4.13 ± 0.07	114.1 ± 0.5	4.081 ± 0.024	114.48 ± 0.17

The distributions of P and θ in the *B*, *V*, *R*, and *I* bands are shown in Figure 1 for all observed stars. The value of P was found in the range of 0.12%–4.46% for the *B*, *V*, *R*, and *I* bands for all stars. However, for the majority of stars, the values of P were found to be in the range of 0.4%–1.4% in all bands. The value of θ is distributed from $52^{\circ}.6$ to $147^{\circ}.8$ in the *B*, *V*, *R*, and *I* bands. The weighted mean values of P and θ were found to be $0.77 \pm 0.01\%$ and $84^{\circ}.4 \pm 0^{\circ}.1$, $0.70 \pm 0.01\%$ and $75^{\circ}.2 \pm 0^{\circ}.2$, $0.76 \pm 0.01\%$ and $74^{\circ}.9 \pm 0^{\circ}.1$, and $0.96 \pm 0.02\%$ and $83^{\circ}.7 \pm 0^{\circ}.6$ in the *B*, *V*, *R*, and *I* bands, respectively, for member stars of the cluster Alessi 1.

We have shown the sky projection of polarization vectors in the *V* band for observed stars over the digitized sky survey (DSS⁵) *R*-band image of the cluster Alessi 1 in Figure 2. The polarization vectors are drawn keeping the stars at the center. Observed stars are marked with a blue dot and the polarization vectors are drawn with blue lines. The length of polarization vectors is proportional to the percentage of polarization. A line of the magnitude of 1% polarization value is shown for the reference at the bottom right of Figure 2. The dashed black line indicates the orientation of the projection of the Galactic plane at $b = -13^{\circ}.30$. Most of the polarization vectors were found to be almost parallel to the direction of the Galactic plane. In the majority of polarimetric studies of open clusters, it was found that the alignments of polarization vectors are almost parallel to the direction of the Galactic plane (e.g., Martínez et al. 2004; Medhi et al. 2007, 2010; Vergne et al. 2007; Orsatti et al. 2010; Eswaraiyah et al. 2011), while toward other lines of sight, the second component of the magnetic field was also found, which was slightly inclined to the Galactic plane (Medhi et al. 2008; Eswaraiyah et al. 2012). Davis & Greenstein (1951) suggested the dominant mechanism for alignment of dust grains in the ISM could be the presence of small non-conservative torque produced by paramagnetic relaxation, and that this torque tends to align the short axis of the rapidly spinning grain along the magnetic field. However, there are some other studies where polarization vectors are found to not be aligned with the Galactic plane, indicating the dust experienced perturbation (Ellis & Axon 1978; Vergne et al. 2010, 2018). Thus, the dust grains along the line of sight of the cluster Alessi 1 are possibly aligned by the Galactic magnetic field and are located in an unperturbed place of our Galaxy.

3.1. Membership

3.1.1. Polarimetric Approach

The light coming from distant stars is partially plane polarized, which is thought to be due to dust grains in the ISM. Hence, the degree of polarization of a star depends on

the column density of aligned dust grains that lie in front of the star, if the star is not intrinsically polarized. So, one can infer that, for the member stars of the cluster, the degree of polarization should be the same. If there is a foreground source then the degree of polarization should be lower, as the light coming from the star will face less column density, and if there is a background source then a higher value of polarization is expected depending upon the length of the column density of grains. Hence, a plot of the Stokes parameters Q ($= P \cos 2\theta$) and U ($= P \sin 2\theta$), also known as a Stokes plane, is a useful tool to distinguish cluster members and non-members. The members of the cluster are expected to group together in the plot and non-members are expected to appear scattered. A plot between Stokes parameters with corresponding errors is shown in Figure 3 for all observed passbands. In this plot, one star in the *I* band is not shown, as this was highly scattered. In Figure 3, rectangles show the 1σ boundary from mean values of Q and U . The mean and standard deviation (σ) of the Q and U were derived by fitting the Gaussian function to their distribution. This boundary can be used to differentiate the members and non-members of the cluster. Stars inside this box can be considered probable members of the cluster.

Using these plots, we found 9 common stars that lie inside the 1σ box in all four passbands. Excluding these 9 stars, 20 stars were found to be common in any three bands and 19 stars were found to be common in any two bands inside the boundary of a 1σ box. If we consider those stars within a 1σ box of Q - U plane, which were common at least in any two bands, as a primary step toward separating members, we found a total of 48 stars to be members of the cluster Alessi 1. However, there is a strong possibility that there are non-members among these stars either due to background population or intrinsic polarization of some stars. So this technique cannot be used alone. Medhi & Tamura (2013) have also used polarimetric data to estimate the membership probability of some open clusters. They have seen that the polarimetric method is inaccurate for non-members stars but this can be used to estimate the membership probability for the known member stars with unknown membership probabilities.

3.1.2. Astrometric Approach

A proper motion study is considered a unique technique for deriving the membership information of stars in any cluster. The distributions of μ_{α} , μ_{δ} , and their corresponding errors ($\sigma_{\mu_{\alpha}}$ and $\sigma_{\mu_{\delta}}$), along with G -band magnitude, are shown in Figure 4. Note that toward the fainter limit ($G > 18$), errors in both μ_{α} and μ_{δ} increase sharply and go up to 4 mas yr^{-1} . Therefore, for further analysis, we have taken only those sources that have both a $\sigma_{\mu_{\alpha}}$ and $\sigma_{\mu_{\delta}}$ that are less than 1 mas yr^{-1} . After applying these criteria, 7598 sources out of 11,004 were left. The top left

⁵ <http://archive.eso.org/dss/dss>

Table 2
Observed Degree of Polarization and Position Angle in the *B*, *V*, *R*, and *I* Bands of the Stars toward the Cluster Alessi 1

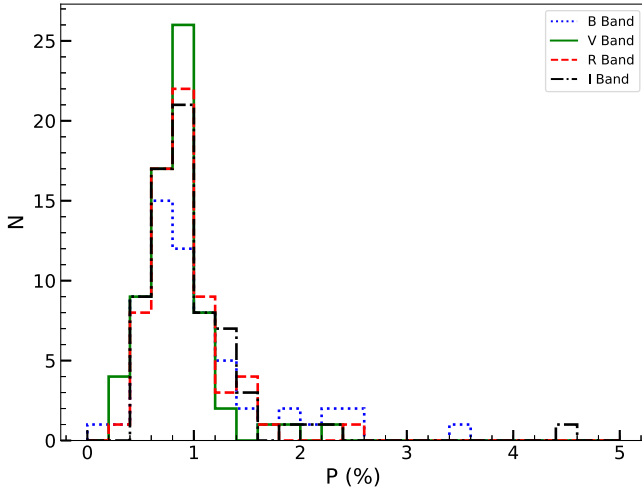
S. No. (1)	Gaia ID (2)	Offset(") (3)	σ (4)	$P_B(\%)$ (5)	$\theta_B(^{\circ})$ (6)	$P_V(\%)$ (7)	$\theta_V(^{\circ})$ (8)	$P_R(\%)$ (9)	$\theta_R(^{\circ})$ (10)	$P_I(\%)$ (11)	$\theta_I(^{\circ})$ (12)
1	414516605226812288	0.89	1.05	0.79 ± 0.08	86.3 ± 2.7	1.12 ± 0.13	87.8 ± 3.3	0.82 ± 0.14	89.0 ± 4.8	0.75 ± 0.05	86.4 ± 2.2
2	402506987611296640	0.69	0.81	0.85 ± 0.16	71.2 ± 5.3	0.83 ± 0.01	100.6 ± 0.3	0.94 ± 0.11	79.1 ± 0.1	0.59 ± 0.11	75.5 ± 0.1
3	402508465080046208	0.32	0.38	2.28 ± 0.79	109.8 ± 9.9	1.35 ± 0.04	85.1 ± 0.9	1.47 ± 0.05	83.3 ± 1.1	1.16 ± 0.46	71.6 ± 11.3
4	402506575294438272	0.16	0.19	2.57 ± 0.01	92.5 ± 0.1	1.02 ± 0.02	82.5 ± 0.7	0.61 ± 0.30	78.9 ± 14.5	1.81 ± 0.46	112.6 ± 7.2
5	402508533799522176	0.67	0.79	1.28 ± 0.05	92.9 ± 1.3	1.82 ± 0.01	76.0 ± 0.1
6	402508739958066048	0.83	0.97	0.86 ± 0.03	82.3 ± 1.1	0.86 ± 0.12	76.7 ± 4.6	0.69 ± 0.02	88.0 ± 0.8	1.31 ± 0.07	80.4 ± 1.1
7 ^a	402508185904098688	0.04	0.05	0.83 ± 0.05	77.6 ± 1.7	0.81 ± 0.04	77.1 ± 1.5	0.71 ± 0.07	76.3 ± 3.0	0.65 ± 0.06	90.6 ± 2.7
8	402505888099785344	0.30	0.35	1.92 ± 0.03	74.6 ± 0.5	0.81 ± 0.05	76.9 ± 1.7	1.01 ± 0.23	98.7 ± 6.4	1.03 ± 0.15	101.9 ± 4.3
9 ^a	402505819380310016	0.12	0.14	0.58 ± 0.12	90.4 ± 6.0	0.77 ± 0.11	82.8 ± 0.2	0.95 ± 0.11	84.6 ± 0.1	0.63 ± 0.14	88.2 ± 6.5
10 ^a	402507331208797056	0.10	0.12	0.97 ± 0.38	78.6 ± 11.3	1.07 ± 0.05	75.3 ± 1.3	1.21 ± 0.49	77.3 ± 11.6
11	402507223831424768	0.25	0.29	0.77 ± 0.12	87.0 ± 4.6	0.94 ± 0.09	76.7 ± 2.4	0.67 ± 0.09	76.3 ± 2.9	0.77 ± 0.15	82.0 ± 8.2
12 ^a	402507911026190592	0.15	0.18	0.66 ± 0.01	86.0 ± 0.4	0.44 ± 0.03	89.3 ± 2.5	0.98 ± 0.02	80.1 ± 0.6	0.62 ± 0.03	97.6 ± 1.4
13 ^a	402507537367224064	0.26	0.31	0.70 ± 0.05	88.7 ± 2.0	0.83 ± 0.06	81.6 ± 2.0	0.96 ± 0.12	78.6 ± 0.6	0.68 ± 0.08	83.3 ± 3.6
14 ^a	402507842306714112	0.16	0.19	0.61 ± 0.10	89.7 ± 4.7	0.88 ± 0.06	75.6 ± 2.1	0.82 ± 0.01	84.9 ± 0.1	0.50 ± 0.08	82.7 ± 4.9
15	414519079128682240	2.05	2.41	2.48 ± 0.71	112.8 ± 8.3	0.78 ± 0.39	105.1 ± 14.6	0.72 ± 0.34	85.0 ± 13.4	0.87 ± 0.08	105.6 ± 2.9
16	414894184393561088	0.01	0.02	0.42 ± 0.01	88.2 ± 0.5	0.56 ± 0.21	87.6 ± 10.4	0.51 ± 0.01	78.2 ± 0.8	0.51 ± 0.01	92.8 ± 0.1
17	414518980347187840	3.91	4.58	0.66 ± 0.03	90.6 ± 1.6	0.80 ± 0.03	85.7 ± 1.3	1.14 ± 0.14	80.3 ± 3.7
18	0.98 ± 0.31	89.5 ± 8.8	1.11 ± 0.30	85.1 ± 7.5	1.11 ± 0.13	88.7 ± 3.3	0.83 ± 0.05	84.8 ± 1.9
19	414518327512167552	3.84	4.50	2.33 ± 0.01	84.3 ± 0.1	0.95 ± 0.11	89.0 ± 3.2	0.71 ± 0.24	108.0 ± 9.7	1.19 ± 0.11	92.6 ± 2.8
20	414518739829026944	2.58	3.03	3.58 ± 0.69	77.1 ± 5.5	2.30 ± 0.06	72.7 ± 0.7	2.49 ± 0.26	83.6 ± 3.0	4.46 ± 1.83	80.9 ± 12.0
21 ^a	414518877267971456	0.89	1.05	0.47 ± 0.21	73.9 ± 12.5	0.65 ± 0.21	77.3 ± 9.3	0.95 ± 0.06	73.6 ± 1.7
22	414518808548492800	0.05	0.06	0.63 ± 0.08	98.8 ± 3.9	0.75 ± 0.02	81.1 ± 0.9	1.05 ± 0.03	84.1 ± 0.8	0.70 ± 0.10	85.1 ± 4.3
23	414894154331125248	0.84	0.98	1.05 ± 0.03	100.8 ± 0.9	1.14 ± 0.31	91.3 ± 7.5	0.99 ± 0.15	81.7 ± 4.5	0.60 ± 0.12	86.4 ± 5.6
24	402884601136206208	3.53	4.13	0.26 ± 0.02	107.1 ± 2.3	0.34 ± 0.02	77.7 ± 2.2	1.66 ± 0.24	85.1 ± 4.1	0.97 ± 0.01	72.2 ± 0.4
25	402884596838415360	3.01	3.53	0.85 ± 0.03	94.4 ± 1.0	0.51 ± 0.11	97.1 ± 0.1	0.70 ± 0.25	103.3 ± 10.1
26	402509113617033088	0.17	0.20	0.62 ± 0.11	69.5 ± 0.7	0.53 ± 0.11	91.0 ± 0.1	0.61 ± 0.20	82.6 ± 9.4	0.72 ± 0.10	86.8 ± 4.1
27	0.42 ± 0.01	61.0 ± 0.3	1.44 ± 0.67	79.0 ± 13.2	2.26 ± 0.05	80.6 ± 0.6
28	402884360618046976	3.82	4.48	1.02 ± 0.14	93.2 ± 4.1	1.63 ± 0.29	78.0 ± 5.0	1.35 ± 0.14	75.9 ± 2.9	1.29 ± 0.08	86.0 ± 1.8
29	402884360618048000	3.79	4.45	0.48 ± 0.11	61.3 ± 0.5	0.62 ± 0.11	81.5 ± 0.3	0.86 ± 0.03	72.2 ± 1.0	0.68 ± 0.04	84.8 ± 2.0
30	402884218880832640	2.09	2.45	0.55 ± 0.05	91.6 ± 2.9	0.64 ± 0.04	83.6 ± 1.8	0.43 ± 0.02	85.7 ± 1.5	0.64 ± 0.13	91.3 ± 6.1
31	402508838740252288	1.47	1.72	1.00 ± 0.38	82.9 ± 10.6	0.91 ± 0.16	108.4 ± 5.0	1.45 ± 0.36	79.5 ± 7.2
32	402884257538834176	2.88	3.37	0.63 ± 0.01	84.7 ± 0.5	1.30 ± 0.01	88.3 ± 0.1
33	1.67 ± 0.49	111.4 ± 8.4	0.80 ± 0.17	93.2 ± 6.2	1.20 ± 0.16	68.6 ± 3.9
34	414520835773063808	1.51	1.77	0.54 ± 0.05	72.8 ± 3.1	1.07 ± 0.10	74.0 ± 2.8	0.85 ± 0.15	79.0 ± 4.9	0.51 ± 0.15	75.9 ± 8.8
35	414520423456212864	0.29	0.34	0.84 ± 0.09	87.3 ± 3.0	0.91 ± 0.06	88.3 ± 2.0	0.57 ± 0.11	85.4 ± 0.4	0.56 ± 0.09	77.0 ± 4.7
36	414520320376999936	1.90	2.23	0.96 ± 0.35	89.8 ± 10.5	1.21 ± 0.31	77.8 ± 7.3	0.90 ± 0.07	71.9 ± 2.3	1.56 ± 0.28	66.3 ± 5.2
37	414518018274513920	3.75	4.39	1.33 ± 0.04	95.1 ± 0.8	0.92 ± 0.02	86.5 ± 0.6	0.94 ± 0.19	76.0 ± 5.7	0.48 ± 0.04	93.4 ± 2.5
38	414517846475834112	1.15	1.35	0.51 ± 0.11	72.8 ± 0.1	1.49 ± 0.26	72.4 ± 5.1	1.28 ± 0.11	113.8 ± 0.1
39	414517812116098816	0.13	0.15	0.62 ± 0.07	86.5 ± 3.5	1.03 ± 0.02	85.2 ± 0.7	0.79 ± 0.12	84.0 ± 1.0	0.72 ± 0.06	87.7 ± 2.7
40	414517228000553984	1.57	1.85	1.12 ± 0.32	53.7 ± 8.0	0.98 ± 0.21	98.3 ± 6.3
41	414517605957672064	0.06	0.07	0.56 ± 0.13	89.0 ± 6.9	0.70 ± 0.01	86.9 ± 0.2	1.00 ± 0.17	63.5 ± 5.0	0.62 ± 0.09	87.7 ± 4.4
42	414516811385241600	0.26	0.31	0.69 ± 0.10	89.6 ± 4.4	0.84 ± 0.04	86.0 ± 1.3	0.63 ± 0.07	80.5 ± 3.2	0.61 ± 0.14	87.2 ± 6.8
43	414519186505623936	3.83	4.49	1.87 ± 0.02	103.4 ± 0.3	0.93 ± 0.01	79.3 ± 0.2	0.93 ± 0.09	74.3 ± 2.7	0.92 ± 0.01	93.1 ± 0.2
44	414518430591386496	2.59	3.04	0.80 ± 0.01	87.7 ± 0.4	0.60 ± 0.11	76.5 ± 0.3	0.56 ± 0.07	81.7 ± 3.8
45	414516300287631616	0.29	0.34	1.30 ± 0.05	96.9 ± 1.2	0.66 ± 0.17	78.4 ± 7.5	0.68 ± 0.04	73.8 ± 1.6	0.88 ± 0.26	93.8 ± 8.6
46	0.65 ± 0.01	88.2 ± 0.1	0.40 ± 0.05	77.2 ± 4.0	0.55 ± 0.03	68.1 ± 1.8	0.77 ± 0.07	85.7 ± 2.7
47 ^a	414516437726588800	0.05	0.06	0.66 ± 0.11	87.9 ± 0.1	0.45 ± 0.13	67.3 ± 8.5	0.47 ± 0.11	72.4 ± 0.3	0.71 ± 0.18	83.0 ± 7.5

Table 2
(Continued)

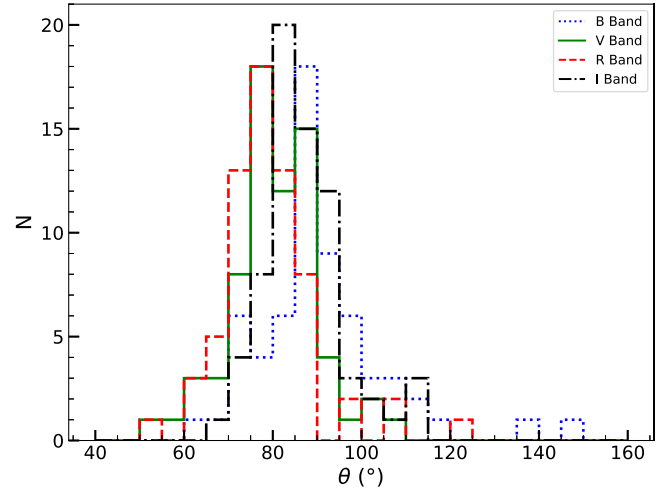
S. No. (1)	Gaia ID (2)	Offset(") (3)	σ (4)	P_B (%) (5)	θ_B ($^\circ$) (6)	P_V (%) (7)	θ_V ($^\circ$) (8)	P_R (%) (9)	θ_R ($^\circ$) (10)	P_I (%) (11)	θ_I ($^\circ$) (12)
48 ^a	402506369136008832	0.06	0.08	0.69 ± 0.05	95.6 ± 2.1	0.69 ± 0.06	67.3 ± 2.6	0.86 ± 0.15	82.1 ± 5.2
49 ^a	402506162977579648	0.05	0.06	0.85 ± 0.04	98.1 ± 1.4	0.82 ± 0.05	78.5 ± 1.9	1.02 ± 0.15	91.8 ± 3.6
50	402506128617841920	0.22	0.26	0.82 ± 0.15	84.7 ± 6.3	0.69 ± 0.05	84.4 ± 0.2	0.71 ± 0.07	70.1 ± 1.2	0.99 ± 0.07	81.5 ± 2.1
51 ^a	402505991178890752	0.15	0.17	0.86 ± 0.18	88.0 ± 6.2	0.65 ± 0.03	73.6 ± 1.5	0.65 ± 0.11	67.8 ± 4.9	0.89 ± 0.15	88.2 ± 5.0
52	402505991178891136	0.16	0.19	1.15 ± 0.13	86.4 ± 3.2	0.54 ± 0.07	83.9 ± 2.1	0.96 ± 0.08	73.8 ± 2.4
53 ^a	402500317524014976	0.15	0.18	1.01 ± 0.14	87.1 ± 4.2	0.70 ± 0.07	75.2 ± 3.1	0.50 ± 0.10	78.3 ± 7.4	1.30 ± 0.17	80.5 ± 4.1
54	402500390541534848	0.35	0.41	0.79 ± 0.07	93.2 ± 2.8	0.64 ± 0.03	73.6 ± 1.5	0.80 ± 0.11	71.1 ± 0.1	0.92 ± 0.05	90.9 ± 1.7
55	414515887970782592	0.08	0.10	0.83 ± 0.10	61.3 ± 3.5	1.14 ± 0.37	83.0 ± 9.4	0.92 ± 0.05	90.9 ± 1.7
56	414516158550216320	0.07	0.09	0.95 ± 0.01	83.3 ± 0.3	0.94 ± 0.01	77.0 ± 0.5	0.86 ± 0.05	62.9 ± 1.8	1.22 ± 0.36	77.1 ± 8.5
57 ^a	414509978093147136	0.16	0.19	1.04 ± 0.02	81.0 ± 0.7	0.79 ± 0.03	72.2 ± 1.3	0.87 ± 0.11	72.3 ± 0.4	1.08 ± 0.19	79.1 ± 5.1
58	414510149894478080	0.08	0.09	1.36 ± 0.11	77.1 ± 0.1	0.86 ± 0.05	72.1 ± 1.9	1.01 ± 0.16	72.2 ± 4.6	0.88 ± 0.29	114.6 ± 9.6
59	1.00 ± 0.38	89.3 ± 11.0	0.61 ± 0.07	84.4 ± 3.6	0.74 ± 0.02	76.8 ± 1.0	0.97 ± 0.13	81.3 ± 4.0
60	402499291029914752	2.76	3.24	1.06 ± 0.25	84.7 ± 6.9	0.86 ± 0.02	64.2 ± 0.7	0.86 ± 0.07	73.5 ± 2.6	0.93 ± 0.19	73.3 ± 6.0
61	402499256670177536	2.97	3.48	2.01 ± 0.48	73.4 ± 6.8	0.86 ± 0.29	96.4 ± 9.8	1.45 ± 0.15	79.5 ± 3.1
62	402500012584419840	2.04	2.39	1.36 ± 0.35	95.4 ± 7.5	0.95 ± 0.13	69.5 ± 4.0	0.80 ± 0.03	64.0 ± 1.3	1.11 ± 0.15	81.1 ± 3.9
63	402500012584421120	1.95	2.29	1.52 ± 0.10	109.3 ± 2.0	0.87 ± 0.23	88.4 ± 7.6	0.63 ± 0.06	120.0 ± 2.7	1.11 ± 0.23	84.0 ± 6.0
64	402505334045815680	2.29	2.69	0.79 ± 0.14	91.2 ± 5.2	0.67 ± 0.11	89.9 ± 4.7	0.45 ± 0.01	93.6 ± 1.0
65	402506059898367104	1.55	1.82	0.36 ± 0.04	66.0 ± 3.1	1.29 ± 0.20	77.0 ± 4.4	0.80 ± 0.28	81.8 ± 10.2
66	402507670508022784	0.14	0.16	0.88 ± 0.24	81.6 ± 7.8	0.88 ± 0.16	76.8 ± 5.3	0.86 ± 0.01	87.4 ± 0.1
67 ^a	402507571726963968	0.19	0.22	0.64 ± 0.03	75.3 ± 1.3	0.75 ± 0.10	78.9 ± 3.8	0.91 ± 0.02	88.0 ± 0.8
68	402504788588155264	0.11	0.13	0.48 ± 0.07	147.8 ± 4.4	0.52 ± 0.18	101.4 ± 10.1	0.25 ± 0.08	89.9 ± 8.8	0.89 ± 0.26	84.9 ± 8.4
69	402879825133045760	0.20	0.23	0.12 ± 0.01	139.5 ± 3.3	0.36 ± 0.02	58.5 ± 1.8	0.89 ± 0.08	73.6 ± 2.6	0.66 ± 0.15	91.5 ± 6.6
70	402504754228418688	0.11	0.13	1.45 ± 0.46	116.2 ± 9.6	0.89 ± 0.21	77.6 ± 7.0	1.37 ± 0.02	69.9 ± 0.4	2.16 ± 0.20	84.2 ± 2.6
71 ^a	402880684126058880	0.07	0.08	0.53 ± 0.07	101.4 ± 3.7	0.87 ± 0.12	85.1 ± 4.0
72	402883291167896832	0.27	0.31	0.80 ± 0.11	93.4 ± 3.9	0.25 ± 0.02	52.6 ± 3.0	0.77 ± 0.11	83.8 ± 4.1	0.94 ± 0.02	96.7 ± 0.6
73	402883428606850816	0.87	1.02	1.05 ± 0.19	72.4 ± 5.2	0.85 ± 0.08	71.6 ± 2.7	1.41 ± 0.14	77.6 ± 3.0	1.16 ± 0.01	80.0 ± 0.3

Note.

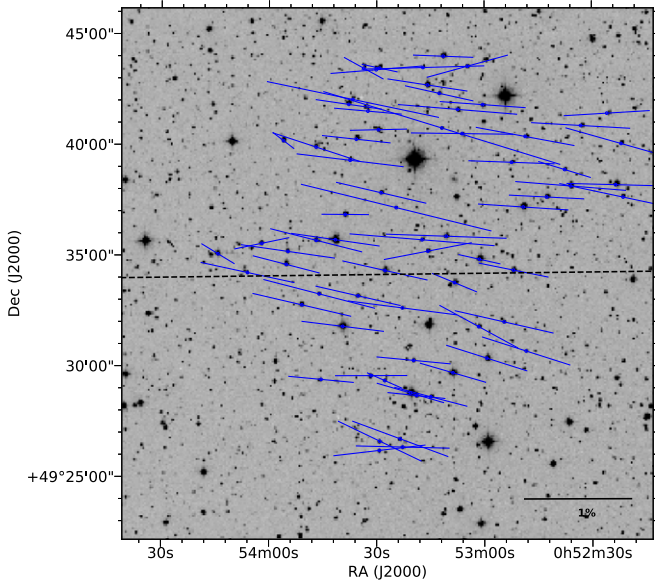
^a Member stars of the cluster Alessi 1. S.No. 18, R.A.:13.279948, decl.:49.693928. S.No. 27, R.A.:13.389086, decl.:49.724924. S.No. 33, R.A.:13.106471, decl.:49.691115. S.No. 46, R.A.:13.254734, decl.:49.581148. S.No. 59, R.A.:13.438451, decl.:49.490717.



(a) Histogram of degree of polarization



(b) Histogram of angle of polarization

Figure 1. Distribution of degree of polarization and position angle of observed stars in the *B*, *V*, *R*, and *I* bands toward the cluster Alessi 1.

Figure 2. Stellar polarization in the *V* band superimposed on a $24' \times 24'$ DSS image of the field containing Alessi 1. The length of the polarization vectors is proportional to P_V . A line of magnitude of 1% polarization value is drawn for reference. The dashed black line indicates the orientation of the projection of the Galactic plane at $b = -13^\circ30'$.

panel of Figure 5 shows the plot between μ_α and μ_δ [also called a vector point diagram (VPD)] of stars in the specified fov. In this plot, there is a small clustering of stars near the central coordinate (μ_α, μ_δ) of $(6.50, -6.28)$ mas yr $^{-1}$. The central values of μ_α and μ_δ were estimated by fitting the Gaussian in their distribution. The bottom left panel of Figure 5 shows the corresponding CMD, where we could not identify any clear sequence of stars. To find the real cluster members, we have plotted VPD with different radii (1 mas yr $^{-1}$ and onward) with center coordinates as mentioned above. The corresponding CMD was also plotted to identify any cluster sequence. We found that by increasing the radius of the circle beyond 1 mas yr $^{-1}$ in VPD, only the number of field stars increased, while no notable increment was seen in the main-sequence stars. So, we constrain ourselves to a 1 mas yr $^{-1}$ radius of the circle in VPD

to define the membership criteria. The chosen radius in VPD is a tradeoff between losing cluster members and including field stars or vice versa. From this approach, we have identified 66 stars as cluster members. The middle panels of Figure 5 show the VPD and CMD for member stars, whereas the right top and bottom panels of this figure show the VPD and CMD of field stars. In the middle CMD, stars in the main sequence are well separated. Using the *Gaia* DR2 data at a $25.5'$ radius from the central coordinate of the cluster Alessi 1, Cantat-Gaudin et al. (2018) estimated a (μ_α, μ_δ) of $(6.536, -6.245)$ mas yr $^{-1}$ and a distance of 704.8 pc. While deriving the membership probability, they have taken only those sources for which $G \leq 18$, typical astrometric uncertainties < 0.3 mas yr $^{-1}$ in proper motion, and parallax uncertainty ≤ 0.15 mas. Out of the 66 members identified by us, 40 stars have membership probability $> 50\%$ as given by Cantat-Gaudin et al. (2018).

3.1.3. Members in the Observed Region

Out of 66 stars identified as members of the cluster Alessi 1, only 15 stars have been observed polarimetrically. These 15 stars share a similar degree of polarization, as they are among the 48 stars that were considered probable members of the cluster from the polarimetric approach. The small fraction of polarimetrically observed stars that we found is due to the small observed field, and does not consider the stars fainter than a *G*-band magnitude of 15 due to large errors, and the locations of stars at the edge of the observed fov and/or due to overlapping of one's ordinary image with another's extraordinary image. In Table 2, these member stars are marked with footnote "a." Thus, similar to the conclusion drawn by Medhi & Tamura (2013), we also conclude that polarimetry alone cannot be used to determine the membership of a cluster.

3.2. Cluster Parameters

Figure 6 shows the CMD of all 66 member stars along with the best-matched isochrones from Marigo et al. (2017). The isochrone with an age of 0.79 Gyr was found to be the best-matched isochrone, whereas isochrones with ages of 0.89 and 0.71 Gyr show the upper and lower limits for age estimation.

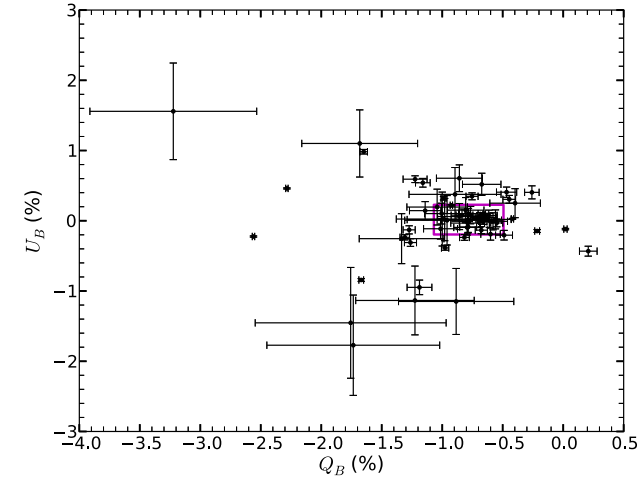
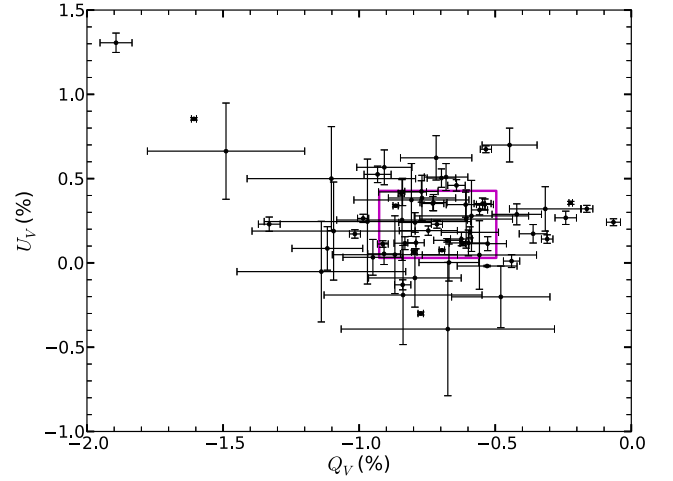
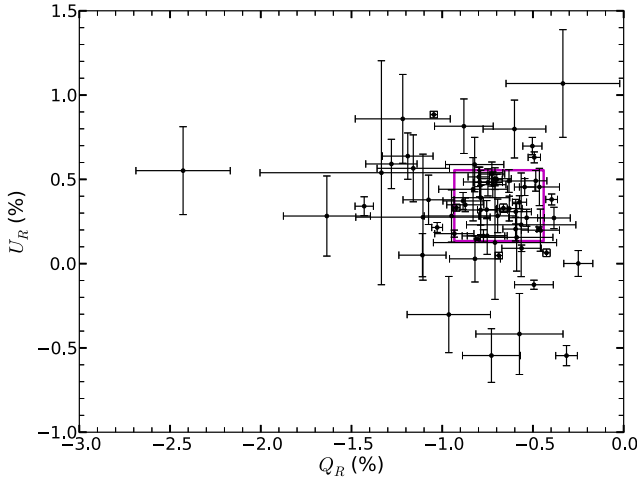
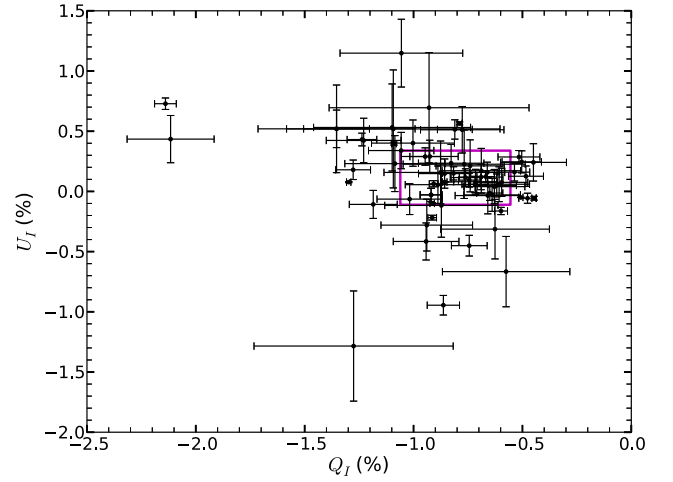
(a) Q versus U in B band(b) Q versus U in V band(c) Q versus U in R band(d) Q versus U in I band

Figure 3. Plot between Stokes parameters Q and U for observed stars in the B , V , R , and I bands. The rectangle in each figure shows the 1σ box from the mean values of Q and U . One star in the I band is far off from the mean values of Q and U , and hence is not shown in the $Q-U$ plot.

Thus, the age of the cluster was estimated as 0.8 ± 0.1 Gyr. Using these isochrones, we have estimated the $E(G_{BP} - G_{RP})$ and distance modulus of the cluster Alessi 1 as 0.23 ± 0.05 mag and 9.6 ± 0.3 mag, respectively. This distance modulus corresponds to a distance of 673 ± 98 pc. While calculating the distance, the extinction in the G band (A_G) was derived using $A_G \approx 2 \times E(G_{BP} - G_{RP})$ (see Andrae et al. 2018) and found to be 0.46 ± 0.10 mag. The age and distance of the cluster that we estimated are very close to those estimated by Kharchenko et al. (2004, 2013) and Bossini et al. (2019).

We have also transformed $(G_{BP} - G_{RP})$ color to $(B - V)$ color using the transformation equation and coefficients of Jordi et al. (2010). A total of 44 stars out of 73 polarimetrically observed stars have $E(G_{BP} - G_{RP})$ in the *Gaia* DR2. Of these, only 18 stars have $E(G_{BP} - G_{RP})$ values with an uncertainty less than 50%. Therefore, for further analysis, we have considered only these 18 stars. We have also transformed $E(G_{BP} - G_{RP})$ to $E(B - V)$ and derived the relation toward that direction of the cluster Alessi 1 as $E(B - V) = 0.7042 \times E(G_{BP} - G_{RP}) + 0.0010$. The

average value of reddening, $E(B - V)$, was thus estimated to be 0.16 ± 0.03 mag. Using the normal reddening law the average value of A_V toward the cluster Alessi 1 is derived to be 0.50 ± 0.09 mag. Our derived values of $E(B - V)$ are consistent with those given in Kharchenko et al. (2013) and Bossini et al. (2019).

3.3. ISM Polarization

We have checked for ISM polarization for almost all observed stars in the cluster region using the Serkowski polarization relation, which states that the wavelength dependence of ISM polarization follows the following empirical law (Serkowski et al. 1975):

$$P_\lambda = P_{\max} \times \exp[-K \times \ln^2(\lambda_{\max}/\lambda)]. \quad (5)$$

Here, P_λ is the degree of polarization measured at a wavelength λ , and λ_{\max} is the wavelength at which maximum polarization P_{\max} occurs. λ_{\max} is a function of the optical properties and characteristic particle size distribution of aligned grains (Carrasco et al. 1973; McMillan 1978; Wilking et al. 1980). K is the inverse

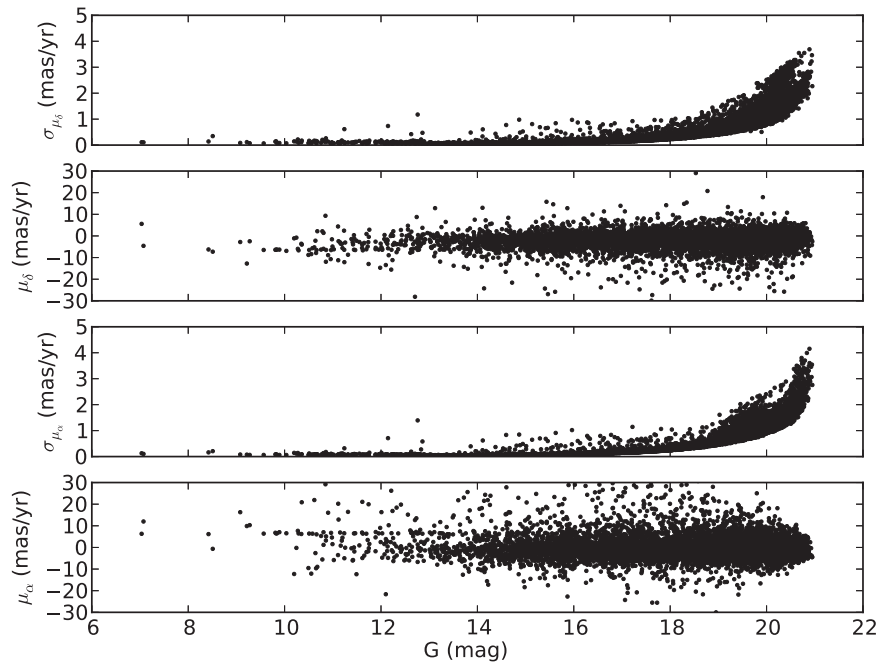


Figure 4. Plot of proper motions and their errors as a function of G -band magnitude.

of the width of the polarization curve and is taken as 1.15 for all stars (Serkowski et al. 1975). The criteria for ISM polarization are well represented by the parameter σ_1 , which is the unit weight error of fit and quantifies the departure of our data from the Serkowski relation. If the polarization curve is well represented by a Serkowski empirical law, the value σ_1 should be less than 1.6 and polarization can be considered due to an ISM origin. The value of σ_1 more than 1.6 and/or a small value of λ_{\max} may indicate the presence of intrinsic polarization. The values of λ_{\max} and P_{\max} have been derived by fitting the observed polarization in the B , V , R , and I passbands to the Serkowski empirical law. The best-fit values of P_{\max} and λ_{\max} , along with the σ_1 for 47 stars, are given in Table 3. We have not included those stars for which errors in the parameters P_{\max} and/or λ_{\max} were found to be greater than 50% of the parameters' values. For the majority of stars, σ_1 was found to be <1.6 , indicating that the polarization toward the Alessi 1 cluster is mainly due to the foreground interstellar dust grains. However, for three non-member stars (S. No. 6, 24, and 43 in Table 3) the value of σ_1 was found to be more than 1.6, which indicates that these stars feature a non-interstellar component in their measured polarization. Also, for some stars the value of λ_{\max} was derived to be outside the range of observed wavelengths even for the stars for which $\sigma_1 < 1.6$. This could be due to the intrinsic polarization of these sources (see also Serkowski et al. 1975). As the exact nature of these stars is not available to us such that we can relate their intrinsic polarization with the properties of the star. Considering member stars of the cluster Alessi 1, we have derived the mean values of λ_{\max} and P_{\max} as $0.59 \pm 0.04 \mu\text{m}$ and $0.83 \pm 0.03\%$, respectively. For the polarization, which is dominated by dust particles present in the diffuse ISM, the value of λ_{\max} lies nearly at $0.55 \mu\text{m}$. The value of λ_{\max} varies from 0.45 to $0.8 \mu\text{m}$ (Serkowski et al. 1975) toward different lines of sight in the ISM. Furthermore, the mean value of λ_{\max} for the cluster Alessi 1 was found to be similar to that found for the location of Alessi 1 in the distribution of λ_{\max} along with the galactic longitude and latitude in the galactic plane. However, at the galactic latitude near -13° , the distribution of

λ_{\max} is not available (see Serkowski et al. 1975). Therefore, the present observations are useful to fill this gap.

Figure 7 is a plot of P/P_{\max} and λ_{\max}/λ . The black curve denotes the Serkowski polarization relation for the general ISM. The Serkowski law for the general ISM was found to be consistent with our observations. We have also calculated the value of total to selective extinction toward the cluster Alessi 1 using the equation $R_V = 5.6 \times \lambda_{\max}$ (Whittet & van Breda 1978). The value of R_V toward the line of sight of the cluster Alessi 1 was found to be 3.3 ± 0.2 , which is similar to the normal reddening law, $R_V = 3.1$. This indicates that the observed polarizations for the stars in the field of the cluster Alessi 1 are mainly due to the ISM and the sizes of dust grains are similar to the general ISM grain sizes.

3.4. Polarization Efficiency

The polarization efficiency is the maximum polarization produced by a given amount of extinction and is measured by the ratio of P_{\max} to the extinction A_V . It depends on the magnetic field strength, the magnetic field's orientation, and the degree of alignment of dust grains along the line of sight (see e.g., Voshchinnikov & Das 2008). For the diffused ISM, the upper limit on the polarization efficiency can be estimated by the relation $P_{\max} < 3.0A_V \approx 3R_V \times E(B - V)$ (Hiltner 1956). Considering the normal reddening law and the average value of $E(B - V)$ for the cluster Alessi 1, the upper limit of P_{\max} was estimated to be 1.5%, which is more than the average value of P_{\max} derived from the Serkowski law for the member stars. Figure 8 shows a polarization efficiency diagram toward the cluster Alessi 1. In Figure 8(a) we show the variation of P_{\max} with $E(B - V)$, where the straight line shows the line of maximum efficiency for $R_V = 3.1$. Here, most of the stars are located below the maximum efficiency line. This indicates that net polarization efficiency is due to the ISM. In Figure 8(b), we have plotted $P_{\max}/E(B - V)$ as a function of $E(B - V)$. As $E(B - V)$ increases, polarization efficiency was found to decrease. A similar trend was also observed for other

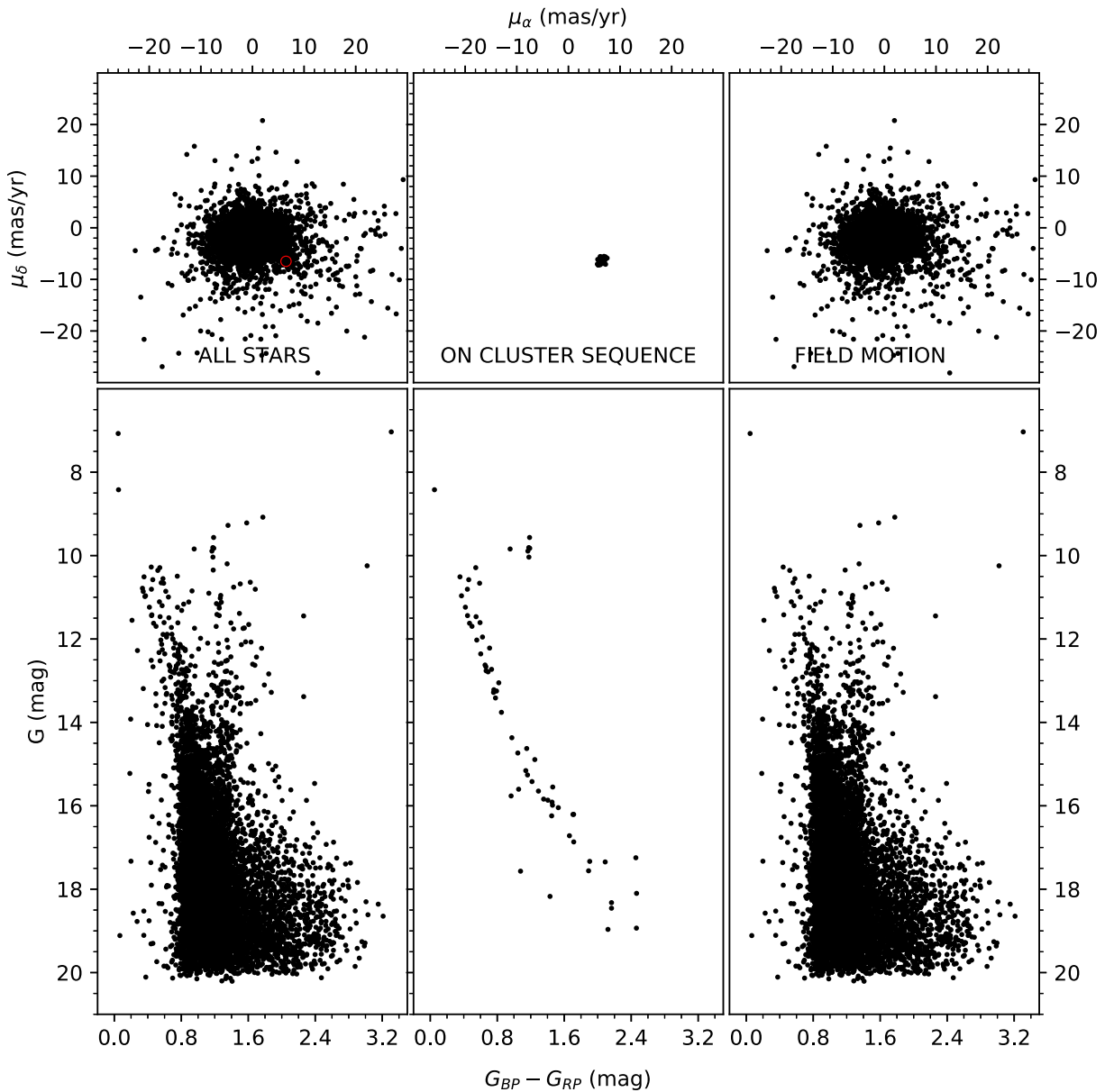


Figure 5. VPD and CMD are shown for stars with proper motion errors $< 1 \text{ mas yr}^{-1}$, around a $26'$ radius of cluster center. A circle of 1 mas yr^{-1} around the cluster centroid in the VPD defines the criterion for membership. The left, middle, and right panels show all stars, only member stars, and the field stars, respectively.

clusters where polarization was found to be due to an ISM origin (Medhi et al. 2008, 2010). This could be due to an increase in the dust grain size or a small change in position angle.

3.5. Distribution of Interstellar Matter

In order to see the distribution of extinction in the cluster Alessi 1, we have used recent extinction maps of Green et al. (2019) in that region. They have presented a new three-dimensional map of dust reddening based on *Gaia* parallaxes and stellar photometry from the Panoramic Survey Telescope and Rapid Response System and the Two Micron All-Sky Survey covering the sky north of a decl. of -30° (three-quarters of the sky), out to a distance of several kiloparsecs. We have accessed their map using the available Python package dust maps (Green 2018) for the polarimetrically observed region of the cluster Alessi 1. The polarization vectors in the V

band were overplotted on the extinction map and are shown in Figure 9(a). The color bar on the right side of the figure shows the range of A_V from 0 to 0.8. The reference polarization vector for 1% polarization is shown at the bottom of the figure. The extinction toward the region of the cluster Alessi 1 appears to be the same. We do not see any highly extinct region toward this direction. Hence, the origin of polarization must be due to dichroic extinction of starlight by ISM dust grains, as almost all polarization vectors are aligned in the same direction.

It is important to know the distribution of polarization to determine the distribution of interstellar matter toward the particular line of sight. If the radiation from the star encounters to the dust layer at a certain distance then the value of polarization will show a sudden jump at that distance. From this, one can infer the number of dust layers encountered by radiation of the star along the path and also can get an idea about foreground dust concentration toward that line of sight

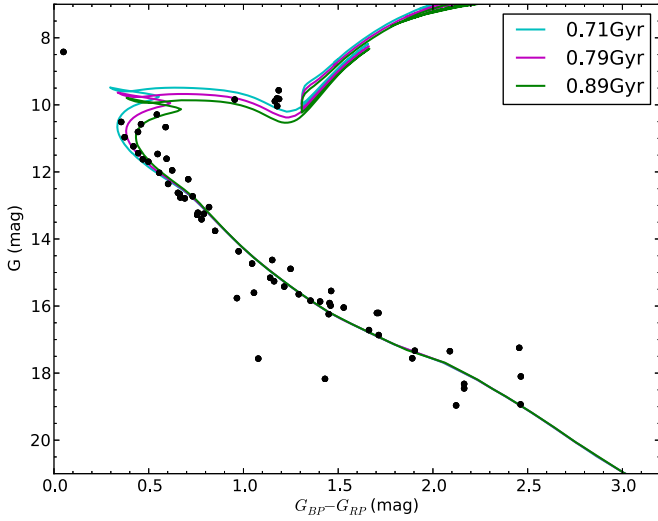


Figure 6. CMD of the member stars of the cluster Alessi 1, along with the best-matched isochrones.

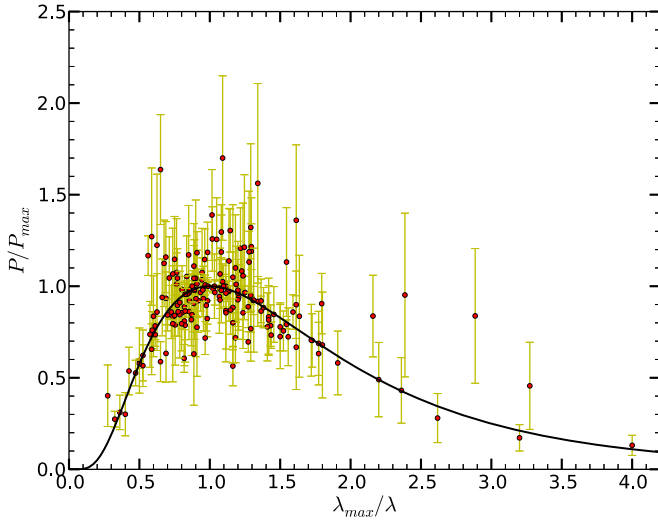


Figure 7. Plot of P/P_{\max} and λ_{\max}/λ . The curve denotes the Serkowski polarization relation for general diffuse ISM.

(e.g., Medhi et al. 2008, 2010; Eswaraiyah et al. 2011). Figure 9(b) show the variation of degree of polarization in the V band with distance. We have also plotted the V -band polarization of the stars from the catalog of Heiles (2000) within a radius of 5° around Alessi 1 cluster. The distances of these stars were taken from the *Gaia* DR2 catalog. The polarization was found to be almost constant at around 0.8% with distance. This indicates that no major dust layer is located along the direction of the cluster. The polarization versus distance diagram for many open clusters shows several sudden increments in the value of polarization, indicating the presence of several dust layers in front of them (e.g., Medhi et al. 2008; Eswaraiyah et al. 2011, 2012). Also, using the $Q-U$ diagram, several dust layers were found to present in front of the open clusters (e.g., Waldhausen et al. 1999; Martínez et al. 2004; Vergne et al. 2007, 2010, 2018; Feinstein et al. 2008). If we take the case of the cluster Be 59, which is the closest observed cluster for polarization to the Alessi 1, three layers of dust are found to present in front of it (Eswaraiah et al. 2012).

Table 3
Values of P_{\max} , λ_{\max} , σ_1 , Membership Probability (MP), and Color Excess $E(B - V)$ for Stars in the Region of the Cluster Alessi 1

S. No. ^a	P_{\max} (%)	λ_{\max} (μm)	σ_1	MP	$E(B - V)$
1	0.89 ± 0.07	0.56 ± 0.07	0.5
2	0.90 ± 0.09	0.47 ± 0.07	0.3
3	1.46 ± 0.06	0.59 ± 0.18	0.8
6	0.80 ± 0.14	0.52 ± 0.22	1.9	...	0.17
7 ^b	0.83 ± 0.02	0.49 ± 0.03	0.2	0.9	0.33
9 ^b	0.80 ± 0.10	0.66 ± 0.15	0.5	0.9	...
10 ^b	1.16 ± 0.08	0.72 ± 0.08	0.2	1.0	0.10
11	0.82 ± 0.09	0.53 ± 0.14	0.5	...	0.44
12 ^b	0.78 ± 0.14	0.64 ± 0.16	1.5	1.0	...
13 ^b	0.81 ± 0.05	0.60 ± 0.06	0.4	0.5	...
14 ^b	0.85 ± 0.08	0.52 ± 0.13	0.6	0.5	0.42
16	0.53 ± 0.01	0.68 ± 0.01	0.1
17	0.96 ± 0.24	0.78 ± 0.19	0.7
18	1.13 ± 0.07	0.49 ± 0.03	0.2
22	0.81 ± 0.09	0.66 ± 0.12	0.5
23	1.06 ± 0.03	0.42 ± 0.03	0.3
24	1.98 ± 0.82	1.76 ± 0.38	1.7	...	0.21
26	0.69 ± 0.07	0.71 ± 0.12	0.3
28	1.35 ± 0.06	0.67 ± 0.06	0.5
29	0.76 ± 0.11	0.78 ± 0.15	0.3
30	0.60 ± 0.07	0.59 ± 0.11	0.4
34	0.81 ± 0.27	0.71 ± 0.28	0.9	...	0.13
35	0.90 ± 0.14	0.42 ± 0.09	0.5
37	1.75 ± 0.23	0.26 ± 0.02	0.4
39	0.79 ± 0.07	0.63 ± 0.10	0.5
41	0.72 ± 0.04	0.62 ± 0.12	0.5
42	0.71 ± 0.06	0.50 ± 0.08	0.3
43	1.10 ± 0.29	0.48 ± 0.19	4.1
44	0.76 ± 0.16	0.46 ± 0.11	0.3
45	2.19 ± 0.65	0.22 ± 0.04	0.8
46	0.66 ± 0.01	0.45 ± 0.12	1.1
47 ^b	0.58 ± 0.11	0.50 ± 0.20	0.6	1.0	0.26
48 ^b	0.75 ± 0.08	0.60 ± 0.11	0.5	0.9	...
49 ^b	0.88 ± 0.07	0.55 ± 0.10	0.7	1.0	...
50	0.98 ± 0.19	0.95 ± 0.18	0.6
51 ^b	0.76 ± 0.12	0.68 ± 0.23	0.6	0.8	...
54	0.92 ± 0.06	0.70 ± 0.09	0.5
55	0.94 ± 0.03	0.76 ± 0.08	0.4
56	0.96 ± 0.01	0.47 ± 0.02	0.6
57 ^b	0.96 ± 0.11	0.54 ± 0.15	0.6	...	0.29
59	1.05 ± 0.29	1.05 ± 0.23	0.7
60	0.89 ± 0.06	0.57 ± 0.13	0.4
62	1.00 ± 0.16	0.71 ± 0.25	0.8
64	0.78 ± 0.03	0.40 ± 0.01	0.1
66	0.90 ± 0.01	0.66 ± 0.01	0.1
70	3.18 ± 1.32	1.44 ± 0.30	0.9	...	0.26
73	1.16 ± 0.03	0.79 ± 0.14	0.8	...	0.31

Notes.

^a The S. No. in this table are similar to those in the Table 2.

^b Member stars of the cluster Alessi 1. Membership probabilities are taken from Cantat-Gaudin et al. (2018) and $E(B - V)$ were estimated from *Gaia* $E(G_{BP} - G_{RP})$.

4. Summary

We have carried out a polarimetric study of 73 stars toward the cluster Alessi 1. The age, distance, and $E(B - V)$ of the cluster Alessi 1 are estimated to be 0.8 ± 0.1 Gyr, 673 ± 98 pc, and 0.16 ± 0.03 mag, respectively, using the archival data from *Gaia*. A total of 66 stars are found to be members of the cluster Alessi 1

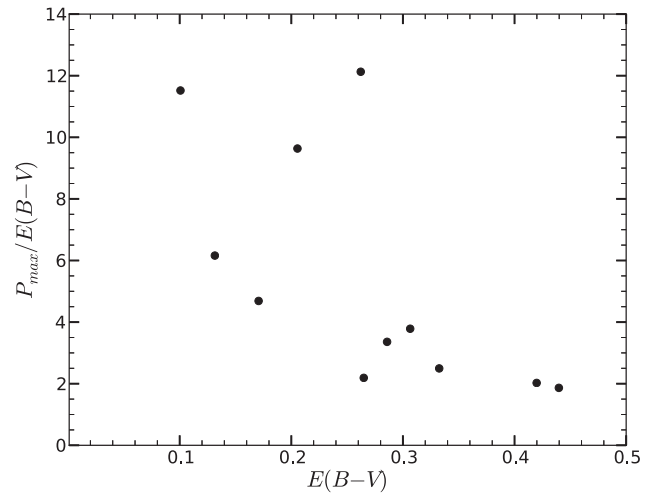
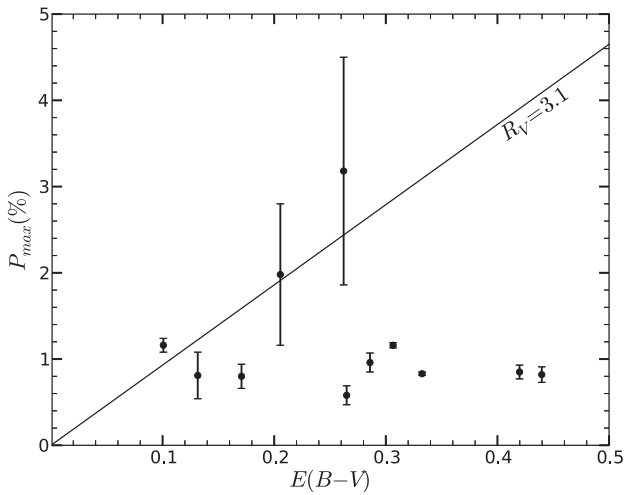
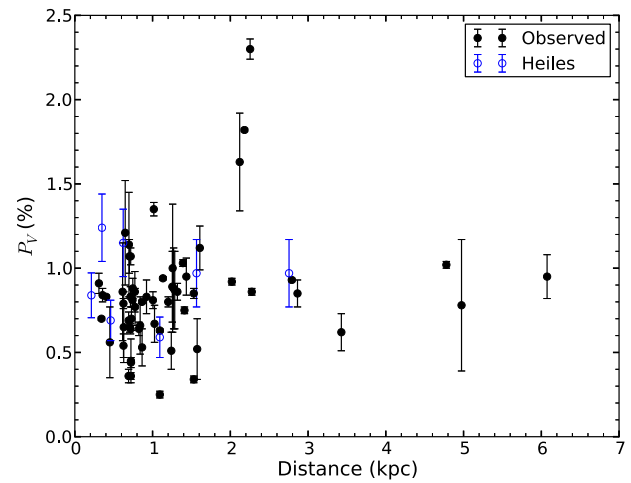
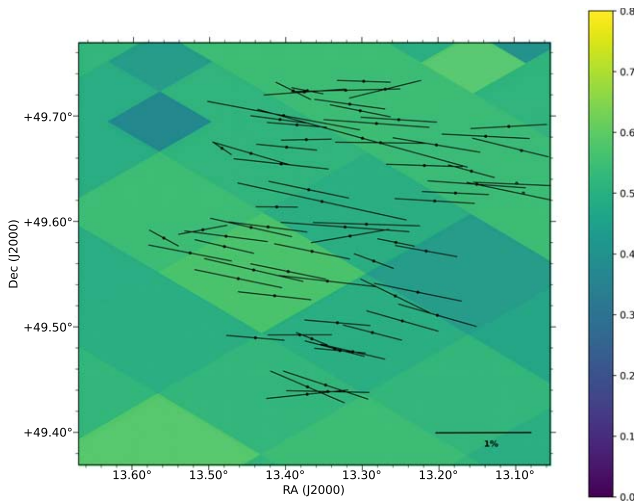


Figure 8. (a) The polarization efficiency curve. The maximum efficiency line using $R_V = 3.1$ is drawn. (b) $P_{\max}/E(B - V)$ plotted as a function of $E(B - V)$.



(a) Polarization vectors over-plotted on extinction map

(b) Distance versus polarization

Figure 9. (a) Extinction map of the cluster Alessi 1 region produced using the Python package dust maps (Green 2018). The color scale on the right denotes the scale for values of A_V for the region. We have overplotted V -band polarization results using vectors. The reference for the polarization vector of 1% polarization is shown at bottom. (b) Variation of degree of polarization in the V band with distance.

using an astrometric approach, out of which 15 member stars are observed polarimetrically. The average value of P and θ for member stars of the cluster Alessi 1 are found to be $0.77 \pm 0.01\%$ and $84^\circ 4 \pm 0^\circ 1$, $0.70 \pm 0.01\%$ and $75^\circ 2 \pm 0^\circ 2$, $0.76 \pm 0.01\%$ and $74^\circ 9 \pm 0^\circ 1$, and $0.96 \pm 0.02\%$ and $83^\circ 7 \pm 0^\circ 6$ in the B , V , R , and I bands, respectively. The distribution of the dust grain toward the direction of Alessi 1 is found to be similar as general ISM as λ_{\max} is found to be $0.59 \pm 0.04 \mu\text{m}$. The average value of maximum polarization is found to be $0.83 \pm 0.03\%$ when considering only the member stars. It is found that polarization toward the Alessi 1 cluster is dominated by foreground dust grains, which are probably aligned by the Galactic magnetic field.

We thank the referee for reading our paper and the useful comments. Part of this work has made use of data from the European Space Agency (ESA) mission *Gaia* (<https://www.cosmos.esa.int/gaia>), processed by the *Gaia* Data Processing and Analysis Consortium (DPAC, <https://www.cosmos.esa.int/web/gaia/dpac/consortium>). Funding for the DPAC has been provided by national institutions, in particular, the institutions participating

in the *Gaia* Multilateral Agreement. This research made use of the cross-match service provided by CDS, Strasbourg.

ORCID iDs

Jeewan C. Pandey  <https://orcid.org/0000-0002-4331-1867>

References

- Alessi, B. S., Moitinho, A., & Dias, W. S. 2003, *A&A*, 410, 565
 Andrae, R., Fouesneau, M., Creevey, O., et al. 2018, *A&A*, 616, A8
 Bossini, D., Vallenari, A., Bragaglia, A., et al. 2019, *A&A*, 623, A108
 Cantat-Gaudin, T., Jordi, C., Vallenari, A., et al. 2018, *A&A*, 618, A93
 Carrasco, L., Strom, S. E., & Strom, K. M. 1973, *ApJ*, 182, 95
 Davis, L., Jr., & Greenstein, J. L. 1951, *ApJ*, 114, 206
 Ellis, R. S., & Axon, D. J. 1978, *Ap&SS*, 54, 425
 Eswaraiyah, C., Pandey, A. K., Maheswar, G., et al. 2011, *MNRAS*, 411, 1418
 Eswaraiyah, C., Pandey, A. K., Maheswar, G., et al. 2012, *MNRAS*, 419, 2587
 Feinstein, C., Vergne, M. M., Martínez, R., & Orsatti, A. M. 2008, *MNRAS*, 391, 447
 Frisch, P. C., Berdyugin, A. B., Pirola, V., et al. 2018, arXiv:1806.02806
 Gaia Collaboration, Brown, A. G. A., Vallenari, A., et al. 2018, *A&A*, 616, A1

- Gaia Collaboration, Prusti, T., de Bruijne, J. H. J., et al. 2016, *A&A*, **595**, A1
- Green, G. M. 2018, *JOSS*, **3**, 695
- Green, G. M., Schlafly, E. F., Zucker, C., Speagle, J. S., & Finkbeiner, D. P. 2019, *ApJ*, **887**, 93
- Heiles, C. 1996, *ApJ*, **462**, 316
- Heiles, C. 2000, *AJ*, **119**, 923
- Hiltner, W. A. 1956, *ApJS*, **2**, 389
- Jordi, C., Gebran, M., Carrasco, J. M., et al. 2010, *A&A*, **523**, A48
- Kharchenko, N. V., Piskunov, A. E., Röser, S., Schilbach, E., & Scholz, R.-D. 2004, *AN*, **325**, 740
- Kharchenko, N. V., Piskunov, A. E., Röser, S., Schilbach, E., & Scholz, R. D. 2005, *A&A*, **438**, 1163
- Kharchenko, N. V., Piskunov, A. E., Schilbach, E., Röser, S., & Scholz, R.-D. 2013, *A&A*, **558**, A53
- Kim, S.-H., & Martin, P. G. 1994, *ApJ*, **431**, 783
- Lazarian, A. 2003, *JQSRT*, **79**, 881
- Lazarian, A. 2007, *JQSRT*, **106**, 225
- Lazarian, A., Goodman, A. A., & Myers, P. C. 1997, *ApJ*, **490**, 273
- Lindgren, L., Hernández, J., Bombrun, A., et al. 2018, *A&A*, **616**, A2
- Luri, X., Brown, A. G. A., Sarro, L. M., et al. 2018, *A&A*, **616**, A9
- Marigo, P., Girardi, L., Bressan, A., et al. 2017, *ApJ*, **835**, 77
- Martínez, R., Vergne, M. M., & Feinstein, C. 2004, *A&A*, **419**, 965
- McMillan, R. S. 1978, *ApJ*, **225**, 880
- Medhi, B. J., Maheswar, G., Brijesh, K., et al. 2007, *MNRAS*, **378**, 881
- Medhi, B. J., Maheswar, G., Pandey, J. C., Kumar, T. S., & Sagar, R. 2008, *MNRAS*, **388**, 105
- Medhi, B. J., Maheswar, G., Pandey, J. C., Tamura, M., & Sagar, R. 2010, *MNRAS*, **403**, 1577
- Medhi, B. J., & Tamura, M. 2013, *MNRAS*, **430**, 1334
- Orsatti, A. M., Feinstein, C., Vergne, M. M., Martínez, R. E., & Vega, E. I. 2010, *A&A*, **513**, A75
- Pandey, J. C., Medhi, B. J., Sagar, R., & Pandey, A. K. 2009, *MNRAS*, **396**, 1004
- Patel, M. K., Pandey, J. C., Karmakar, S., Srivastava, D. C., & Savanov, I. S. 2016, *MNRAS*, **457**, 3178
- Rautela, B. S., Joshi, G. C., & Pandey, J. C. 2004, *BASI*, **32**, 159
- Schmidt, G. D., Elston, R., & Lupie, O. L. 1992, *AJ*, **104**, 1563
- Serkowski, K., Mathewson, D. S., & Ford, V. L. 1975, *ApJ*, **196**, 261
- Sinvhal, S. D., Kandpal, C. D., Mahra, H. S., Joshi, S. C., & Srivastava, J. B. 1972, in *Optical Astronomy with Moderate Size Telescopes*, ed. R. V. Karandikar, K. Alladin, & S. Sastry (Naini Tal: Uttar Pradesh State Obs.), 20
- Soam, A., Kwon, J., Maheswar, G., Tamura, M., & Lee, C. W. 2015, *ApJL*, **803**, L20
- Vaillancourt, J. E., Dowell, C. D., Jones, T. J., et al. 2011, in *EAS Publ. Ser. 52, Conditions and Impact of Star Formation*, ed. M. Röellig et al. (Les Ulis: EDP Sciences), 259
- Vergne, M. M., Feinstein, C., & Martínez, R. 2007, *A&A*, **462**, 621
- Vergne, M. M., Feinstein, C., Martínez, R., Orsatti, A. M., & Alvarez, M. P. 2010, *MNRAS*, **403**, 2041
- Vergne, M. M., Feinstein, C., & Martínez, R. E. 2018, *RMxAA*, **54**, 293
- Voshchinnikov, N. V. 2012, *JQSRT*, **113**, 2334
- Voshchinnikov, N. V., & Das, H. K. 2008, *JQSRT*, **109**, 1527
- Waldhausen, S., Martínez, R. E., & Feinstein, C. 1999, *AJ*, **117**, 2882
- Whittet, D. C. B., & van Breda, I. G. 1978, *A&A*, **66**, 57
- Wilking, B. A., Lebofsky, M. J., Martin, P. G., Rieke, G. H., & Kemp, J. C. 1980, *ApJ*, **235**, 905